A LETTERS JOURNAL EXPLORING
THE FRONTIERS OF PHYSICS

OFFPRINT

Dynamics of a nanoscale rotor driven by single-electron tunneling

Alexander Croy and Alexander Eisfeld

EPL, **98** (2012) 68004

Please visit the new website
`www.epljournal.org`

epl

A Letters Journal Exploring
the Frontiers of Physics

AN INVITATION TO
SUBMIT YOUR WORK

www.epljournal.org

The Editorial Board invites you to submit your letters to EPL

EPL is a leading international journal publishing original, high-quality Letters in all areas of physics, ranging from condensed matter topics and interdisciplinary research to astrophysics, geophysics, plasma and fusion sciences, including those with application potential.

The high profile of the journal combined with the excellent scientific quality of the articles continue to ensure EPL is an essential resource for its worldwide audience. EPL offers authors global visibility and a great opportunity to share their work with others across the whole of the physics community.

Run by active scientists, for scientists

EPL is reviewed by scientists for scientists, to serve and support the international scientific community. The Editorial Board is a team of active research scientists with an expert understanding of the needs of both authors and researchers.

epl
A Letters Journal Exploring
the Frontiers of Physics

epl
A Letters Journal Exploring
the Frontiers of Physics

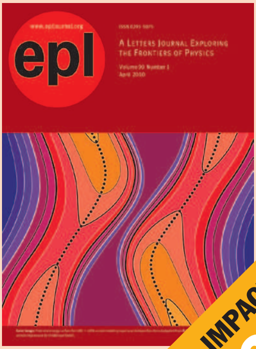
epl
A Letters Journal Exploring
the Frontiers of Physics

IMPACT FACTOR
2.753*
* As ranked by ISI 2010

www.epljournal.org

epl A LETTERS JOURNAL EXPLORING THE FRONTIERS OF PHYSICS

www.epljournal.org

IMPACT FACTOR
2.753*
* As listed in the ISI® 2010 Science Citation Index Journal Citation Reports

OVER
500 000
full text downloads in 2010

30 DAYS
average receipt to online publication in 2010

16 961
citations in 2010
37% increase from 2007

"We've had a very positive experience with EPL, and not only on this occasion. The fact that one can identify an appropriate editor, and the editor is an active scientist in the field, makes a huge difference."

Dr. Ivar Martinv
Los Alamos National Laboratory, USA

Six good reasons to publish with EPL

We want to work with you to help gain recognition for your high-quality work through worldwide visibility and high citations.

1. **Quality** – The 40+ Co-Editors, who are experts in their fields, oversee the entire peer-review process, from selection of the referees to making all final acceptance decisions
2. **Impact Factor** – The 2010 Impact Factor is 2.753; your work will be in the right place to be cited by your peers
3. **Speed of processing** – We aim to provide you with a quick and efficient service; the median time from acceptance to online publication is 30 days
4. **High visibility** – All articles are free to read for 30 days from online publication date
5. **International reach** – Over 2,000 institutions have access to EPL, enabling your work to be read by your peers in 100 countries
6. **Open Access** – Articles are offered open access for a one-off author payment

Details on preparing, submitting and tracking the progress of your manuscript from submission to acceptance are available on the EPL submission website **www.epletters.net**.

If you would like further information about our author service or EPL in general, please visit **www.epljournal.org** or e-mail us at **info@epljournal.org**.

EPL is published in partnership with:

European Physical Society

Società Italiana di Fisica

EDP Sciences

IOP Publishing

www.epljournal.org

epl

A LETTERS JOURNAL
EXPLORING THE FRONTIERS
OF PHYSICS

EPL Compilation Index

www.epljournal.org

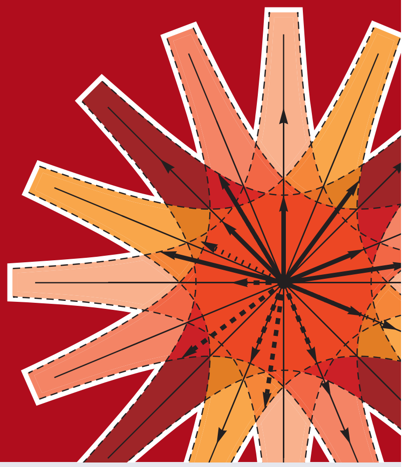

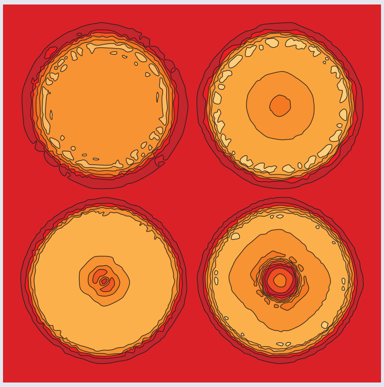

Biaxial strain on lens-shaped quantum rings of different inner radii, adapted from **Zhang *et al*** 2008 EPL **83** 67004.

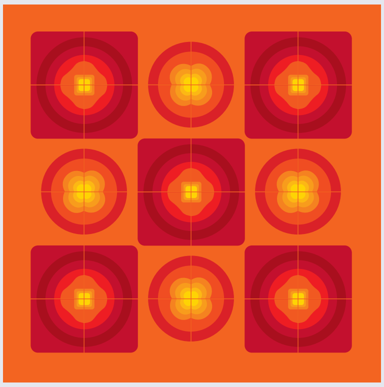

Artistic impression of electrostatic particle–particle interactions in dielectrophoresis, adapted from **N Aubry and P Singh** 2006 *EPL* **74** 623.

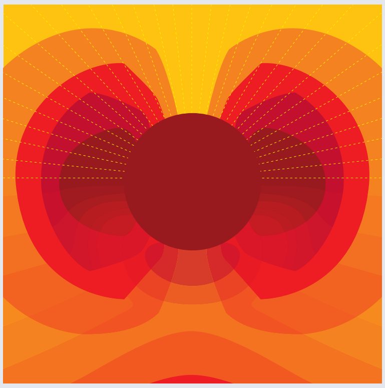

Artistic impression of velocity and normal stress profiles around a sphere that moves through a polymer solution, adapted from **R Tuinier, J K G Dhont and T-H Fan** 2006 *EPL* **75** 929.

Visit the EPL website to read the latest articles published in cutting-edge fields of research from across the whole of physics.

Each compilation is led by its own Co-Editor, who is a leading scientist in that field, and who is responsible for overseeing the review process, selecting referees and making publication decisions for every manuscript.

- Graphene
- Liquid Crystals
- High Transition Temperature Superconductors
- Quantum Information Processing & Communication
- Biological & Soft Matter Physics
- Atomic, Molecular & Optical Physics
- Bose–Einstein Condensates & Ultracold Gases
- Metamaterials, Nanostructures & Magnetic Materials
- Mathematical Methods
- Physics of Gases, Plasmas & Electric Fields
- High Energy Nuclear Physics

If you are working on research in any of these areas, the Co-Editors would be delighted to receive your submission. Articles should be submitted via the automated manuscript system at **www.epletters.net**

If you would like further information about our author service or EPL in general, please visit **www.epljournal.org** or e-mail us at **info@epljournal.org**

EPS

Società Italiana
di Fisica

EDP
SCIENCES

IOP Publishing

Image: Ornamental multiplication of space-time figures of temperature transformation rules (adapted from T. S. Bíró and P. Ván 2010 *EPL* **89** 30001; artistic impression by Frédérique Swist).

A Letters Journal Exploring
the Frontiers of Physics

June 2012

EPL, **98** (2012) 68004
doi: 10.1209/0295-5075/98/68004

www.epljournal.org

Dynamics of a nanoscale rotor driven by single-electron tunneling

Alexander Croy[1,2(a)] and Alexander Eisfeld[1,3(b)]

[1] *Max-Planck-Institute for the Physics of Complex Systems - Nöthnitzer Str. 38, 01187 Dresden, Germany, EU*
[2] *Department of Applied Physics, Chalmers University of Technology - 41296 Göteborg, Sweden, EU*
[3] *Department of Chemistry and Chemical Biology, Harvard University - 12 Oxford Street, Cambridge, MA 02138, USA*

received 3 January 2012; accepted in final form 23 May 2012
published online 25 June 2012

PACS 85.85.+j – Micro- and nano-electromechanical systems (MEMS/NEMS) and devices
PACS 85.35.-p – Nanoelectronic devices

Abstract – We investigate theoretically the dynamics and the charge transport properties of a rod-shaped nanoscale rotor, which is driven by a similar mechanism as the *nanomechanical single-electron transistor (NEMSET)*. We show that a static electric potential gradient can lead to self-excitation of oscillatory or continuous rotational motion. We identify the relevant parameters of the device and study the dependence of the dynamics on these parameters. We discuss how the dynamics are related to the measured current through the device. Notably, in the oscillatory regime we find a negative differential conductance. The current-voltage characteristics can be used to infer details of the surrounding environment which is responsible for damping.

Copyright © EPLA, 2012

Introduction. – In recent years it has emerged that the coupling of electrical and mechanical degrees of freedom on the nanometer scale provides the opportunity to build novel devices, extending the concepts of conventional electronic devices [1,2]. A seminal example is the nanomechanical single-electron transistor (NEMSET) [3–6], where electrons can tunnel from a source to a drain electrode via a movable island or grain, whose charge (*i.e.*, the number of excess electrons that occupy the island) is determined by the Coulomb-blockade effect. Since the tunneling amplitude depends exponentially on the position of the island, the current is very sensitive to the mechanical motion. For a sufficiently large bias voltage a self-excitation of periodic oscillations occurs in conjunction with charging and de-charging of the island. This mechanically assisted charge transport is called electron shuttling [3]. The grain is embedded in a medium which creates a restoring force and determines essentially the eigenfrequency of the oscillation of the shuttle.

In this letter we consider a device which can rotate freely and which is driven by the same mechanism as the electron shuttle described above. The driving force is determined by a static voltage which is applied along the device [7–9]. In contrast to the conventional shuttles this results in a force that depends non-linearly on the relevant system coordinate. Moreover, there is no mechanical restoring force in the present case. The coupling of mechanical motion and tunneling leads, as we will show, to the self-excitation of oscillatory and rotational motion even in the presence of damping. The frequency of oscillation (rotation) depends on the ratio of the driving force and the friction.

While being based on the same principle as the charge shuttle, the present device exhibits noticeable differences. In the oscillatory regime, the current through the device decreases with increasing bias voltage, which is surprising from the conventional shuttling point of view. We attribute this effect to the presence of a separatrix in the phase space which separates oscillations from rotations. Approaching the separatrix involves a slowing-down of the dynamics and decreasing oscillation amplitudes, which results in the decreasing current. In the rotational regime, one may realize a nanoscale motor which is driven by a static voltage [9].

Using numerical calculations supplemented by an analytical analysis, we find that the dynamics of the rotor are governed by three dimensionless parameters, namely, tunneling length, field strength and damping constant. This circumstance allows us to predict, for example, a transition from oscillatory to rotational motion fairly independent of the actual realization (*e.g.*, used materials, details of the shape) of the device. Our analysis provides an intuitive picture of the dynamics for a large range of the above parameters. For the specific case in which the rotor is based on the setup of fig. 1(a)

[(a)] E-mail: alexander.croy@chalmers.se
[(b)] E-mail: eisfeld@pks.mpg.de

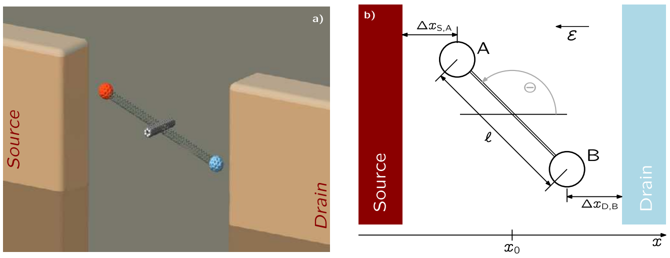

Fig. 1: (Color online) (a) Artistic view of a possible realization of the single-electron motor using (multi-wall) carbon nanotubes and two charge islands. (b) Sketch of the relevant parts and coordinates.

we argue that the interesting oscillatory regime as well as the rotational regime can be obtained with reasonable physical parameters.

Model. – A possible realization of the device, discussed in the present letter, is sketched in fig. 1. It consists of two charge islands (*e.g.*, quantum dots, metallic nanoclusters, etc.), which we denote by A and B, placed at the ends of a rigid rod of length ℓ. This structure can rotate in the (x, y)-plane around an axis in the middle of the rod. The support shaft of the rotor could be realized similarly to the one of ref. [10] by multi-walled carbon nanotubes or in a way proposed in ref. [7]. The motion of the rotor around the pivot axis is characterized by the angle Θ and the corresponding moment of inertia I.

To drive the device, the rotor is placed between source (S) and drain (D) contacts which are connected to electron reservoirs. The contacts are kept at different chemical potentials by an externally applied bias voltage. The electrons may tunnel between the contacts and the charge islands. The respective tunneling amplitudes depend sensitively on the position of the islands. Specifically, we assume an exponential dependence [3]. For example, the tunneling amplitude from the source to island A is $T_{\mathrm{S,A}} \propto \exp[-\Delta x_{\mathrm{S,A}}/\lambda_{\mathrm{S,A}}]$, where $\Delta x_{\mathrm{S,A}}$ is the distance between the source contact and island A and $\lambda_{\mathrm{S,A}}$ is the tunneling length. Similar expressions are used for the tunneling amplitudes $T_{\mathrm{D,A}}$, $T_{\mathrm{S,B}}$ and $T_{\mathrm{D,B}}$. It is convenient to introduce the dimensionless ratio

$$\xi_{\mathrm{S,A}} = \frac{\ell}{\lambda_{\mathrm{S,A}}}\,, \tag{1}$$

which can be regarded as a measure of the change of distance with respect to the tunneling length.

Since the islands are nanoscale objects, their charging will be determined by the Coulomb-blockade effect [11,12]. For sufficiently small tunnel coupling, electrons are transferred sequentially. According to the orthodox theory of Coulomb blockade [11,13,14] the tunneling rates are (for island A)

$$W_{\mathrm{S,A}}(\Theta) = \Gamma_{\mathrm{SA}} \mathrm{e}^{-\xi_{\mathrm{S,A}}\cos(\Theta)}, \tag{2a}$$

$$W_{\mathrm{D,A}}(\Theta) = \Gamma_{\mathrm{DA}} \mathrm{e}^{+\xi_{\mathrm{D,A}}\cos(\Theta)}, \tag{2b}$$

where, for example, Γ_{SA} is defined as the tunneling rate from source to dot A when the rotor is in the perpendicular position, *i.e.*, for $\Theta = \pi/2$. Similar relations hold for the tunneling rates of island B (replacing $\cos(\Theta)$ by $\cos(\Theta + \pi)$).

In the following, we shall consider a very large charging energy such that only one excess electron can occupy each island at the same time (Coulomb-blockade regime). Further, for simplicity, we assume that the bias voltage is very large (large-bias limit). The large-bias approximation holds as long as the respective broadened energy level is completely in the transport window, *i.e.*, for source-drain voltages $eV_{\mathrm{SD}} \gg k_{\mathrm{B}}T$ and $eV_{\mathrm{SD}} \gg \Gamma_{\mathrm{SA/B}} + \Gamma_{\mathrm{DA/B}}$. Here, k_{B} is the Boltzmann constant and T denotes the temperature of the electronic reservoirs. Then electron transport occurs only in one direction [15], *i.e.*, from the source contact electrons can tunnel onto the islands. On the other side of the device they can tunnel from the islands to the drain contact.

Dynamics. – Denoting the electronic population of island A (B) by $P_{\mathrm{A(B)}}$ we can write for average charges of the islands $q_{\mathrm{A(B)}} = -eP_{\mathrm{A(B)}}$, where $P_{\mathrm{A(B)}}$ can attain values between 0 and 1. Due to the tunnel coupling to the leads the populations $P_{\mathrm{A(B)}}$ are time dependent and determined by the rate equation

$$\dot{P}_{\mathrm{A}} = W_{\mathrm{S,A}}(\Theta)\,(1 - P_{\mathrm{A}}) - W_{\mathrm{D,A}}(\Theta) P_{\mathrm{A}}. \tag{3}$$

The first term on the right-hand side describes tunneling from the source onto island A and the second term is responsible for tunneling from the island to the drain contact.

When island A possesses a charge q_{A}, then it experiences a force F_x in the x-direction which is proportional to the electric-field strength $\mathcal{E} \propto V_{\mathrm{SD}}$ induced by the source-drain voltage V_{SD} between the contacts, *i.e.*, $F_x = q_{\mathrm{A}}\,\mathcal{E}$. Then, in the mean-field description introduced above, the torque acting on the rotor is given by $M_{\mathrm{A}} = -e\,P_{\mathrm{A}}\,\mathcal{E}\,\frac{\ell}{2}\,\sin(\Theta)$. A similar expression holds for island B (replacing $\sin(\Theta)$ by $\sin(\Theta + \pi)$).

To keep the discussion transparent, in the following we will take all tunneling rates to be equal[1] and denote them by Γ. This rate can then be used to introduce a dimensionless time,

$$\tau = \Gamma\, t, \tag{4}$$

and a dimensionless field strength,

$$\eta \equiv e\mathcal{E}\ell/(2I\Gamma^2). \tag{5}$$

---

[1] In practice the couplings of the different islands to the two leads will not be perfectly identical. From our numerical simulations we have found that the features discussed in the present work are quite robust with respect to changes in the relative couplings. For example, even for very asymmetric tunneling rates $\Gamma_{\mathrm{SA}}/\Gamma_{\mathrm{DA}} \approx 4$ the results presented in the following remain qualitatively the same.

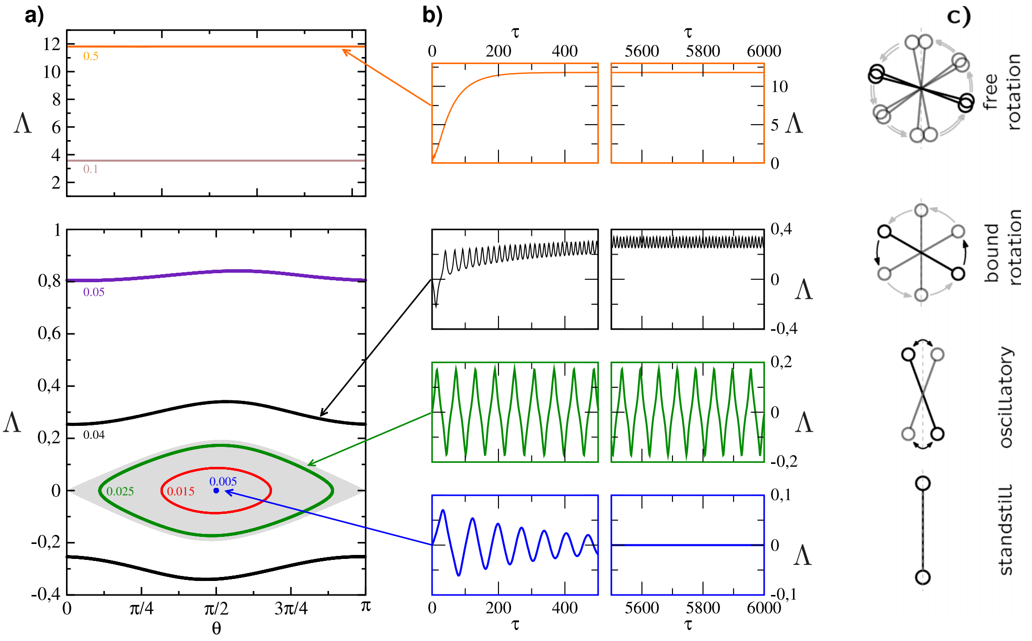

Fig. 2: (Color online) Dynamics of the rotor for various η and fixed $\gamma = 0.01$ and $\xi = 2$. (a) Phase portrait of the steady-state dynamics. Within the gray-shaded area an oscillatory motion takes place. The values of η are given next to the respective trajectory. (b) Examples of the time evolution that leads to the corresponding steady-state dynamics. (c) Sketch of the dynamics for the four cases shown in (b).

Due to the torque $M_A + M_B$ there will be a change in angular momentum L of the rotor. For the dimensionless angular momentum

$$\Lambda = \frac{L}{I\Gamma} \tag{6}$$

the equation of motion reads

$$\begin{aligned}\frac{\partial}{\partial \tau}\Lambda &= -\eta\left(\sin(\Theta)P_A + \sin(\Theta+\pi)P_B\right) - F(\Lambda)\\ &= -\eta\sin(\Theta)\Delta P - F(\Lambda),\end{aligned} \tag{7}$$

where we have added a phenomenological damping term $F(\Lambda)$ and in the last line we have defined $\Delta P = P_A - P_B$. In the following calculations we choose the damping to be linearly dependent on the velocity [7,16], *i.e.*, $F(\Lambda) = \gamma\Lambda$, with a dimensionless damping constant γ. The damping will typically be accompanied by fluctuations, whose influence will be discussed in a later section.

The population difference ΔP, which appears in eq. (7), also depends on time. We have

$$\frac{\mathrm{d}\Delta P}{\mathrm{d}\tau} = -2\sinh[\xi\cos(\Theta)] - 2\cosh[\xi\cos(\Theta)]\Delta P, \tag{8}$$

where we have also set all tunneling lengths equal to ξ.

Finally, the angle Θ is related to the momentum Λ by

$$\frac{\partial\Theta}{\partial\tau} = \Lambda. \tag{9}$$

The three coupled equations, (7), (8) and (9), govern the dynamics of the system. In the following, we will investigate how this dynamics depends on the parameters ξ, γ and η. We are mainly interested in the steady-state dynamics at long times after the initial irregularities have vanished.

For given damping γ and tunneling length ξ we find three qualitatively different regimes of the steady-state motion depending on the values of the driving η. These are illustrated in fig. 2(c). In fig. 2(a), (b) numerical solutions of the set of equations (7)–(9) are shown for $\gamma = 0.01$ and $\xi = 2$.

In fig. 2(a) the steady-state solutions for various values of η are depicted by representing the angular momentum Λ as a function of the angle Θ. Different initial conditions Θ_0 lead to the same steady-state solution apart from the dependence on the direction of rotation, which is opposite for Θ_0 and $-\Theta_0$. In fig. 2(b) examples of the initial time dependence of the angular momentum are shown for a situation where the rotor is initially at rest at an angle $\Theta = 0.4$.

For $\eta < \gamma$ the rotor shows a relaxation towards the equilibrium position given by $\Theta = \pi/2$, *i.e.*, both islands A and B are in the middle between the source and the drain contact. Obviously, in this regime the dynamics of the rotor are dominated by the damping, which leads to the motion of the rotor being slow compared to the tunneling time. Consequently, the populations are in equilibrium with the reservoirs at each instant of time. Additionally, the strong damping leads to decreasing amplitudes and, in the symmetric case considered here,

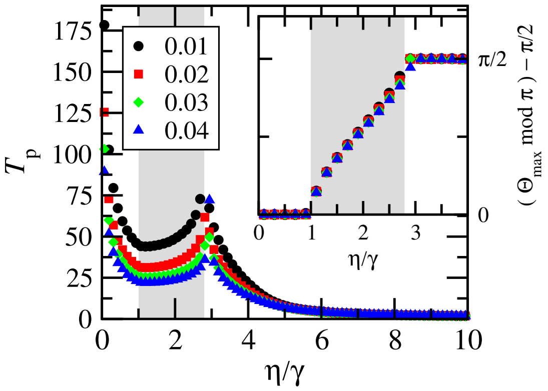

Fig. 3: (Color online) The period of steady-state oscillations/rotations T_p in units of τ is shown as a function of η/γ. Different symbols (colors) indicate different values of γ, as given in the legend. The inset shows the corresponding maximal angle relative to $\Theta = \pi/2$.

the population difference vanishes accordingly. Since the rotor is not accelerated anymore, the motion eventually comes to a halt. Electrons will tunnel with the constant rate Γ to/from the islands to the contacts. The stationary solution is given by the single (blue) point in fig. 2(a), located at $\Theta = \pi/2$ and $\Lambda = 0$.

Upon increasing η one reaches a regime where the rotor oscillates around the position $\Theta = \pi/2$ and the force on the charged islands is not yet strong enough to lead to a rotational motion. This regime is characterized by closed curves within the shaded area in fig. 2(a). The outmost trajectory of this area was obtained from an adiabatic approximation to eq. (8) and by considering extremal swing. The occurrence of the oscillatory regime is a direct consequence of the distance dependence in the tunneling rates. For sufficiently weak damping, inertia leads to slightly increasing amplitudes in each period. Due to the increasing tunneling rates, this is accompanied by an increase of the population difference and, therefore, a larger backward acceleration. Of course the increase of the oscillation amplitude will be limited by the damping, which becomes more and more important as the velocity (or amplitude) increases. Consequently, one has two competing mechanisms: one that favors an increase in the oscillation amplitude (electric field/tunneling) and one that acts to decrease it (damping). The result is the occurrence of stable oscillations in the long-time limit. Notice that these oscillations are akin to the self-excited shuttling in NEMSET [3]. However, in contrast to the conventional charge shuttle, for the rotor the period of the oscillation increases with increasing η. This behavior is illustrated in fig. 3, where the period of steady-state oscillation/rotation is shown as a function of η/γ. In the oscillatory regime, indicated by the gray-shaded area, a clear increase of the period of oscillation can be seen, spiking at $\eta/\gamma \approx 2.8$. This point corresponds to the separatrix as shown in fig. 2(a).

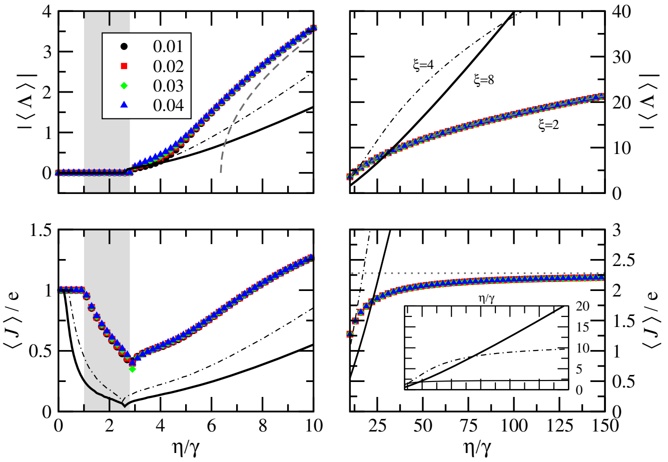

Fig. 4: (Color online) Dependence of the average angular momentum $\langle\Lambda\rangle$ and the average current $\langle J\rangle$ on the ratio η/γ. Symbols denote results for $\xi = 2$ and different values for γ as given in the legend. Right column: focus on large values of η/γ. Left column: details for small η/γ. The dashed line indicates the behavior obtained from eq. (11) and the dotted line shows the asymptotic value of the stationary current $\langle J\rangle_\mathrm{stat} = \Gamma\, I_0(\xi)$. The inset shows $\langle J\rangle$ for the same η/γ, but on a larger scale.

For even larger values of η periodic rotational motion sets in (see the curves for $\eta = 0.04$ and $\eta = 0.05$ in fig. 2(a)). The direction of rotation in the long-time limit depends on the initial conditions. In this regime, the motion is dominated by the driving through the electric field. The rotational energy becomes large enough to overcome the damping and to allow an almost free rotation, characterized by a constant angular momentum. This case is shown in fig. 2(a) in the upper panel.

Angular momentum. – With respect to a possible application as a motor, the temporally averaged angular momentum in the steady state is an important quantity. Thus, in our numerical simulations we calculate

$$\langle\Lambda\rangle = \frac{1}{\mathcal{T}} \int_{t_1}^{t_1+\mathcal{T}} \Lambda(t)\mathrm{d}t, \qquad (10)$$

where we have chosen the time t_1 large enough to ensure that we are in the regime of stationary dynamics and we have taken the time interval $\mathcal{T}$ to cover many periods of oscillation (rotation). In fig. 4 numerical results for various ξ and γ are shown. The different colors of the dots represent different values of γ for the same ξ as in fig. 2. As can be anticipated from eq. (7), with $F(\Lambda) = \gamma\Lambda$, the curves for different values of γ nearly coincide.

In the upper row of fig. 4 the dependence of $|\langle\Lambda\rangle|$ on η/γ is shown. Obviously, in the damping-dominated regime the average angular momentum is zero, since $\Lambda \to 0$ in the stationary limit. Also in the oscillatory regime (indicated by the gray-shaded area) one has $\langle\Lambda\rangle = 0$, since the angular momentum changes its sign in each period (see, *e.g.*, the third row of fig. 2(b)). Thus, the averaged Λ is not an ideal quantity with which to gain insight in the oscillatory regime. However, it is well suited in the rotational regime, which is characterized by a finite value of the average angular momentum $\langle\Lambda\rangle$ and its modulus[2]. In the left column of fig. 4 the focus is on relatively small values of η/γ. In the right column the region from $\eta/\gamma = 10$ to $\eta/\gamma = 150$ is covered. In this region the dependence of the angular momentum on η/γ can be estimated analytically. In the stationary limit, the time averages of the dissipated work and the work due to accelerating the charges have to be equal, *i.e.*, $\langle W_{\text{fric}}\rangle = \langle W_{\text{charge}}\rangle$. Changing the time-average to an angular average leads to $\gamma\int_0^{2\pi}\mathrm{d}\Theta\,\Lambda(\Theta) = -\eta\int_0^{2\pi}\mathrm{d}\Theta\,\Delta P(\Theta)\sin(\Theta)$. For large values of η/γ, the angular momentum is constant, *i.e.*, $\langle\Lambda\rangle \approx \Lambda \equiv \Lambda_{\text{stat}}$. After integration by parts and replacing the resulting derivative of the population difference $\mathrm{d}\Delta P/\mathrm{d}\Theta = (\mathrm{d}P/\mathrm{d}\tau)/(\mathrm{d}\Theta/\mathrm{d}\tau)$ by eq. (8), one obtains

$$\Lambda_{\text{stat}} \approx \sqrt{c(\xi)\frac{\eta}{\gamma} - d(\xi)} \qquad (11)$$

with $c(\xi) = \langle\cos(\Theta)2\sinh(\xi\cos(\Theta))\rangle_\Theta$ and $d(\xi) = \langle\cos(\Theta)2\cosh(\xi\cos(\Theta))\Delta P\rangle_\Theta$. Using the Jacobi-Anger identity, the first term becomes $c(\xi) = 2I_1(\xi)$, where I_n is the n-th order modified Bessel function of the first kind. The second term is more difficult to evaluate. To eliminate the population difference, one has to repeatedly use eq. (8). However, in the limit $\eta/\gamma \to \infty$ this second term vanishes. We have found that these analytical estimates describe our numerical results very well in the region of large η/γ.

Current. – Since the dynamics of the rotor are essentially driven by charge transport it is instructive to take a closer look at the electric current. The time-dependent current (in units of the electron charge e) is given by

$$J(t)/e = W_{\text{A,D}}\big(\Theta(t)\big)\,P_A(t) + W_{\text{B,D}}\big(\Theta(t)\big)\,P_B(t). \qquad (12)$$

As before, we are primarily interested in the time-averaged current $\langle J\rangle$, which we define in the same manner as in eq. (10). Note that the resulting stationary current is independent of the initial condition and, in particular, of the direction of rotation.

Numerical results for $\xi = 2$ are shown in the second row of fig. 4. Here the average current is plotted as a function of η/γ for different γ (the same as for the angular momentum in the upper row). Again, all curves coincide quite well. From the behavior of the averaged current one can clearly distinguish the regime where the rotor oscillates back and forth (corresponding to the shaded area) and the regime corresponding to a motionless rotor ($\eta/\gamma < 1$).

For a very small ratio η/γ the current is constant, since the rotor does not move and electron transport takes place by tunneling to and from the islands in the middle between the contacts. In contrast, in the region where the rotor oscillates one finds a rapid decrease of the average current. When the rotational motion starts, the current rises again slowly. The decrease in the current is related to the fact that the mechanical motion is becoming slower as the separatrix, which separates the oscillation trajectories from the rotating ones, is approached (cf. fig. 3). With increasing η/γ, the amplitude of the oscillations increases and the rotor spends an increasing time at the reversal point, where the tunneling to the opposite electrode is strongly diminished. This results in a decrease of the current.

In the limit of a very large ratio η/γ, the stationary current attains a constant value, which is readily calculated from eqs. (3) and (12) by replacing the rates by their time averages. One obtains $\langle W_{\text{S,A}}\rangle = \Gamma_{\text{SA}}I_0(\xi_{\text{S,A}})$ and $\langle W_{\text{D,A}}\rangle = \Gamma_{\text{DA}}I_0(\xi_{\text{D,A}})$, where $I_0(\xi)$ denotes the modified Bessel function of the first kind. The stationary current (for the case of identical tunnel parameters) is then given by $\langle J\rangle_{\text{stat}} = \Gamma\,I_0(\xi)$. This value is depicted in fig. 4 as the horizontal dotted line. It is in very good agreement with the numerical results.

In addition to the case $\xi = 2$, in fig. 4 numerical results for other values of ξ are shown, too. One sees that for larger ξ the drop in the current sets in for smaller values of η/γ and is more pronounced.

Robustness of the results. – In the following, we comment briefly on the robustness of our results with respect to asymmetries in the couplings to the leads and fluctuations of the environment (*e.g.*, related to internal friction or interaction with some background gas at finite temperature). In the present work we have restricted ourselves to an ideal situation, neglecting these effects, since we wanted to keep our analysis as clear as possible. Our results are only weakly affected by including different couplings and fluctuations. For the couplings this has been discussed when the rate Γ has been introduced. To gain insight into the influence of fluctuations we included a Langevin term $\sqrt{2\gamma\tilde{T}}\zeta(t)$ in eq. (7) and solved the resulting stochastic differential equation numerically (here $\tilde{T} = k_\text{B}T/(I\Gamma^2)$ is the dimensionless temperature and $\zeta(t)$ represents Gaussian white noise). For small η the fluctuations have the largest effect. In the oscillatory regime and close to the separatrix they can lead to sporadic rotations. Similarly, in the standstill regime, oscillations with a few periods can be triggered, resulting in a small decrease of the current. Overall, this leads to a smoothing of the observed features for the time-averaged quantities. However, for moderate fluctuation strengths (approximately smaller than the dissipative energy $\gamma\langle\Lambda\rangle$), the qualitative behavior is not changed. In the rotational regime (large η) our results were, as expected, nearly unaffected by fluctuations.

In the following we will discuss briefly the realizability of the oscillatory regime. From our numerical simulations we have found that the feature of negative differential conductance is well established as long as $\tilde{T} \lesssim 0.005$ (for values of $\gamma \sim 0.1$). Now we describe a set of realistic parameters which meet this condition. For the length of the rotor we take $\ell = 10\,\mathrm{nm}$. Assuming that the rotor consists of a carbon nanotube, capped by two metallic islands, we estimate $I \approx 10^4\,\mathrm{zg\,nm}^2$. The friction coefficient is taken to be $50\,\mathrm{zg\,nm}^2/\mathrm{ps}$. For an operating temperature $T = 100\,\mathrm{mK}$ the required tunneling rates then have to fulfill the condition $\Gamma \gtrsim 5 \times 10^9/\mathrm{s} \equiv \Gamma_0$. The source-drain voltage, estimated from eq. (5), for Γ_0 and $\eta/\gamma \approx 10$ is $V_{\mathrm{SD}} \approx 3 \times 10^{-3}\,\mathrm{V}$. This estimate leads to a field strength $\mathcal{E} \approx 3 \times 10^{-4}\,\mathrm{V/nm}$. These values indicate, that the setup sketched in fig. 1 might provide a possible physical realization of the device discussed in the present work.

---

[2] When considering $\langle\Lambda\rangle$ instead of $|\langle\Lambda\rangle|$ a branching of the curve appears where the upper and lower branches describe anti-clockwise or clockwise rotation, respectively. The direction of rotation depends in a non-trivial way on the initial angle Θ_0. Due to the symmetry of the system, changing Θ_0 to $-\Theta_0$ reverses the direction.

Conclusions. – We have investigated the dynamics of a nanoscale rotor which is driven by the sequential tunneling of electrons between electronic contacts and the rotor device. The interplay of the electric and the mechanical degrees of freedom leads to three different regimes for the motion of the rotor, which can be obtained by adjusting the external bias voltage. These regimes correspond to stationary, oscillatory and rotational motion.

The oscillatory regime has some similarities with the oscillatory motion of the conventional charge shuttles. However, in contrast to the charge shuttles, the motion of the rotor is slowed down with increasing driving strength. This behavior results in a *decrease* of the electric current with *increasing* bias voltage. In the rotational regime the current starts to increase again and the device can be considered as a nanoscale motor. It is worth noting that the setup discussed in the present paper has some similarities with bio-motors [8], such as the F0 motor of adenosine triphosphate synthase. Further examples of molecular rotors can be found in ref. [17].

One might speculate about possible applications of the device presented here. Due to the high sensitivity of the current to the ratio η/γ, the device may be used to detect changes in its environment. For example, the damping constant γ may be determined by tuning the voltage and maintaining the same current. In this scenario the rotor can be used as a sensor. Another possible application is given in the context of electron pumping. Especially in the rotation regime the charge transport is determined by the mechanical motion. This provides the possibility of a mechanically stabilized pumping in the high-frequency regime. In view of recent achievements regarding the cooling of nanomechanical systems to the quantum regime [18–21], the questions as to if and how it is possible to cool a nanomechanical rotor and its interplay with quantum gears [22] will be an interesting subject for further studies.

In summary, the rotor investigated here is an interesting nanoelectromechanical device with potential applications as a sensor or a single-electron motor.

* * *

The authors would like to thank Prof. Ulf Saalmann and John Briggs for their helpful comments during the preparation of the manuscript. AE acknowledges financial support by the DFG under contract No. Ei 872/1-1 and thanks A. Aspuru-Guzik for hospitality.

REFERENCES

[1] Craighead H. G., *Science*, **290** (2000) 1532.

[2] Blencowe M., *Phys. Rep.*, **395** (2004) 159.

[3] Gorelik L. Y., Isacsson A., Voinova M. V., Kasemo B., Shekhter R. I. and Jonson M., *Phys. Rev. Lett.*, **80** (1998) 4526.

[4] Isacsson A., Gorelik L. Y., Voinova M. V., Kasemo B., Shekhter R. I. and Jonson M., *Physica B: Condens. Matter*, **255** (1998) 150.

[5] Shekhter R. I., Galperin Y., Gorelik L. Y., Isacsson A. and Jonson M., *J. Phys.: Condens. Matter*, **15** (2003) R441.

[6] Moskalenko A. V., Gordeev S. N., Koentjoro O. F., Raithby P. R., French R. W., Marken F. and Savel'ev S. E., *Phys. Rev. B*, **79** (2009) 241403.

[7] Wang B., Vuković L. and Král P., *Phys. Rev. Lett.*, **101** (2008) 186808.

[8] Smirnov A. Y., Savel'ev S., Mourokh L. G. and Nori F., *Phys. Rev. E*, **78** (2008) 031921.

[9] Smirnov A., Mourokh L., Savel'ev S. and Nori F., *Proc. SPIE*, **7364** (2009) 73640D.

[10] Fennimore A. M., Yuzvinsky T. D., Han W.-Q., Fuhrer M. S., Cumings J. and Zettl A., *Nature*, **424** (2003) 408.

[11] Averin D. V., Korotkov A. N. and Likharev K. K., *Phys. Rev. B*, **44** (1991) 6199.

[12] Grabert H. and Devoret M. H. (Editors), *Single Charge Tunneling: Coulomb Blockade Phenomena in Nanostructures*, *NATO Sci. Ser. B*, Vol. **294** (Plenum Press) 1992.

[13] Beenakker C. W. J., *Phys. Rev. B*, **44** (1991) 1646.

[14] Meir Y., Wingreen N. S. and Lee P. A., *Phys. Rev. Lett.*, **66** (1991) 3048.

[15] Gurvitz S. A. and Prager Y. S., *Phys. Rev. B*, **53** (1996) 15932.

[16] Cohen D., *J. Phys. A: Math. Gen.*, **27** (1994) 4805.

[17] Kottas G. S., Clarke L. I., Horinek D. and Michl J., *Chem. Rev.*, **105** (2005) 1281.

[18] O'Connell A. D., Hofheinz M., Ansmann M., Bialczak R. C., Lenander M., Lucero E., Neeley M., Sank D., Wang H., Weides M., Wenner J., Martinis J. M. and Cleland A. N., *Nature*, **464** (2010) 697.

[19] Teufel J. D., Donner T., Li D., Harlow J. W., Allman M. S., Cicak K., Sirois A. J., Whittaker J. D., Lehnert K. W. and Simmonds R. W., *Nature*, **475** (2011) 359.

[20] Poot M. and van der Zant H. S. J., *Phys. Rep.*, **511** (2012) 273.

[21] Chan J., Mayer Alegre T. P., Safavi-Naeini A. H., Hill J. T., Krause A., Groeblacher S., Aspelmeyer M. and Painter O., *Nature*, **478** (2011) 89.

[22] MacKinnon A., *Nanotechnology*, **13** (2002) 678.